

# Visualizing Rabi Dynamics in Complex Systems: A Pedagogical Introduction to Rabi Spectra and the Breakdown of the Rotating Wave Approximation

Duje Bonacci, ORCID: 0000-0002-8168-1367\*

Ministry of Science, Education and Youth, Zagreb, Croatia and  
Faculty of Croatian Studies, University of Zagreb, Zagreb, Croatia

(Dated: May 13, 2025)

Rabi oscillations offer a powerful framework for understanding driven transitions in quantum systems, but their textbook form often fails when applied to complex many-level systems or off-resonant fields. In this paper, we introduce the concept of a **Rabi spectrum** — a graphical method for diagnosing when the rotating wave approximation (RWA) is valid, and for estimating the selectivity and speed of population transfer in both simple and complex quantum systems. The approach provides both a conceptual and computational shortcut for determining when the standard two-level solution breaks down. Illustrated with numerical simulations and analytical results, the Rabi spectrum method is presented as a practical tool for both teaching and research.

PACS numbers:

## I. INTRODUCTION

State-selective manipulation of discrete-level quantum systems — such as atoms, molecules, or engineered qubits — is central to a wide range of fields, including laser control of chemical reactions, atom optics, high-precision metrology, and quantum information processing [1–3]. The elementary mechanism enabling such control is often the so-called *Rabi oscillation* — the periodic population transfer between two quantum states under the influence of a coherent, near-resonant external drive. This phenomenon, originally analyzed by I.I. Rabi in the context of nuclear magnetic resonance [4], is now a standard concept in both introductory quantum mechanics and advanced quantum control.

The textbook treatment of Rabi oscillations is appealingly simple, typically relying on the *rotating wave approximation* (RWA). This approximation assumes that the rapidly oscillating terms in the Schrödinger equation can be neglected, yielding a closed-form solution describing sinusoidal population oscillations. While this solution is accurate for weak, near-resonant fields in two-level systems, its limitations become severe when applied to strong fields, off-resonant driving, or — most importantly — to real-world systems with many accessible energy levels.

A number of studies have addressed corrections to the RWA in two-level systems [5–8], including methods to account for the Bloch-Siegert shift or strong-driving effects [9–12]. However, these approaches are often mathematically involved, based on perturbation theory, Floquet analysis, or numerical diagonalization, and therefore less suitable for quick conceptual diagnostics or pedagogical use.

In addition, most analytical approaches to single-laser Rabi dynamics are limited to isolated two-level systems.

This restricts their utility in many-level contexts — such as molecules with dense rovibrational spectra, artificial atoms with multiple excitations, or superconducting transmon qubits with anharmonic ladders [2? ]. In such systems, the presence of nearby states can distort the intended two-level dynamics or introduce significant population leakage, even under weak driving. Yet, there is a surprising lack of simple, general tools for assessing whether a given transition can be effectively and selectively driven in a many-level environment.

This paper aims to fill that gap. In the first section, we present a mathematically simple but rigorous analysis of the conditions under which the RWA holds in two-level systems. In the second, we introduce the concept of the *Rabi profile* — a Lorentzian-like function describing the population transfer amplitude as a function of drive frequency. This graphical tool provides an intuitive and quick way to judge the applicability of RWA without solving differential equations.

In the third and final section, we extend the concept to many-level systems by defining the *Rabi spectrum*: the superposition of Rabi profiles from all transitions coupled by the drive. We show how this spectrum enables visual diagnosis of potential crosstalk, loss channels, and field intensity limits for clean population transfer. The method is validated through numerical simulations on a model three-level system and proposed as a useful teaching and research aid in modern quantum control.

Throughout this paper, we work in atomic units and set  $\hbar = 1$ .

## II. ROTATING WAVE APPROXIMATION IN A TWO-LEVEL SYSTEM

This section provides a pedagogically motivated derivation and interpretation of the rotating wave approximation (RWA) in a driven two-level quantum system.

While the RWA is a staple of introductory treatments

---

\*Electronic address: dbonacci@fhs.unizg.hr

of quantum dynamics, its limitations and the role of counter-rotating terms are often underappreciated. Here, we analyze when and why the RWA holds, and establish a precise criterion that will serve as the foundation for the graphical approach developed later in the paper.

### A. Full dynamical equation

Consider a two-level quantum system described by the time-dependent Schrödinger equation:

$$i \frac{\partial}{\partial t} \psi(\mathbf{x}, t) = (H_0(\mathbf{x}) + V(t)) \psi(\mathbf{x}, t), \quad (1)$$

where  $\mathbf{x}$  denotes spatial coordinates, and  $H_0(\mathbf{x})$  is the unperturbed Hamiltonian with eigenstates and energies:

$$H_0 \phi_i(\mathbf{x}) = E_i \phi_i(\mathbf{x}), \quad (i = 1, 2). \quad (2)$$

The system is driven by a homogeneous monochromatic external field:

$$V(\mathbf{x}, t) = \hat{\sigma}(\mathbf{x}) F_0 \cos(\omega t), \quad (3)$$

where  $\hat{\sigma}(\mathbf{x})$  is a parity-odd operator (e.g., electric dipole),  $F_0$  is the field amplitude, and  $\omega$  is the driving frequency.

Assuming the system starts in a superposition of its two eigenstates, we expand the wavefunction as:

$$\psi(t) = \sum_{i=1}^2 a_i(t) \phi_i(\mathbf{x}) e^{-iE_i t}. \quad (4)$$

Inserting Eq. (4) into Eq. (1) yields coupled differential equations for the amplitudes  $a_i(t)$ :

$$\frac{d}{dt} a_j(t) = -i F_0 \cos(\omega t) \sum_{i=1}^2 a_i(t) I_{ij} e^{-is_{ij}\omega_{ij}t}, \quad j = 1, 2, \quad (5)$$

where  $\omega_{ij} = |E_i - E_j|$ ,  $s_{ij} = \text{sign}(E_i - E_j)$ , and the transition matrix elements are:

$$I_{ij} = \int \phi_i(\mathbf{x}) \hat{\sigma}(\mathbf{x}) \phi_j(\mathbf{x}) d\mathbf{x}. \quad (6)$$

By symmetry,  $I_{12} = I_{21}$  and  $I_{11} = I_{22} = 0$ .

Expanding the cosine in Eq. (5) and rescaling time via

$$\tau \equiv s_{12} \frac{F_0 I_{12}}{2} t, \quad (7)$$

we obtain the dynamics in a convenient matrix form:

$$\frac{d}{d\tau} \mathbf{a}(\tau) = -i \begin{bmatrix} 0 & e^{2i\Gamma\tau} + e^{-2i\Delta\tau} \\ e^{-2i\Gamma\tau} + e^{2i\Delta\tau} & 0 \end{bmatrix} \mathbf{a}(\tau), \quad (8)$$

where:

$$\mathbf{a}(\tau) = \begin{bmatrix} a_1(\tau) \\ a_2(\tau) \end{bmatrix}, \quad (9)$$

and the dimensionless detuning parameters are defined as:

$$\Delta = \frac{\omega - \omega_{12}}{F_0 I_{12}}, \quad \Gamma = \frac{\omega + \omega_{12}}{F_0 I_{12}}. \quad (10)$$

These parameters quantify, respectively, the proximity to resonance and the spectral asymmetry of the driving field. The populations of the two levels are given by  $\Pi_i(t) = |a_i(\tau)|^2$ .

### B. RWA solution and its limitations

The rotating wave approximation assumes that the counter-rotating terms — those containing  $\Gamma$  — in Eq. (8) oscillate so rapidly that they average out over the timescale of the system's evolution. To test this assumption, we retain all terms and proceed analytically.

Differentiating Eq. (8) with respect to  $\tau$  and eliminating  $\frac{d\mathbf{a}}{d\tau}$  using the same equation, we obtain second-order equations for each amplitude:

$$\begin{aligned} \frac{d^2}{d\tau^2} a_{1,2}(\tau) &= 2a_{1,2}(\tau) \\ &\mp \Delta e^{\mp 2i\Delta\tau} a_{2,1}(\tau) \\ &\pm \Gamma e^{\pm 2i\Gamma\tau} a_{2,1}(\tau) \\ &- 2 \cos(2(\Gamma + \Delta)\tau) a_{1,2}(\tau). \end{aligned} \quad (11)$$

This equation is exact. If we retain only the first term on the right-hand side, we recover the textbook RWA solution: sinusoidal population oscillations with period  $\Theta_0 = \pi$  and amplitude  $A_0 = 1$  [14].

Including the second term yields the well-known off-resonant Rabi oscillations, with period and amplitude:

$$\Theta_\Delta = \pi \frac{1}{\sqrt{1 + \Delta^2}}, \quad A_\Delta = \frac{1}{1 + \Delta^2}. \quad (12)$$

The third and fourth terms represent the corrections to RWA. Their importance depends on  $\Gamma$ : if  $\Gamma \gg 1$ , both terms rotate rapidly, but the third dominates due to its prefactor  $\Gamma$ . If  $\Gamma \ll 1$ , the fourth term becomes more relevant despite its lack of a prefactor.

#### 1. Weak Perturbation Case: $\Gamma \gg 1$

Let us focus on the  $\Gamma \gg 1$  regime. Here the perturbation of the driving field is weak in the sense that the coupling strength  $F_0 I_{12}$  is small compared to the transition energy  $\omega_{12}$ , so the counter-rotating terms oscillate rapidly and average out over the timescale of the system's evolution.

The third term introduces the so-called Bloch-Siegert oscillations [15], which appear as small ripples superimposed on the main Rabi oscillations. To estimate their effect, we write the solution as a perturbative sum:

$$\mathbf{a}(\tau) = \mathbf{a}_\Delta(\tau) + \mathbf{a}_\Gamma(\tau), \quad (13)$$

where  $\mathbf{a}_\Delta(\tau)$  is the RWA solution, and  $\mathbf{a}_\Gamma(\tau)$  captures the correction due to the third term.

Inserting into Eq. (8) and linearizing in  $\mathbf{a}_\Gamma$ , we obtain:

$$\mathbf{a}_\Gamma(\tau) \approx -i \int_{\tau_0}^{\tau} \begin{bmatrix} 0 & e^{2i\Gamma\tau} \\ e^{-2i\Gamma\tau} & 0 \end{bmatrix} \mathbf{a}_\Delta(\tau) d\tau. \quad (14)$$

Assuming that  $\mathbf{a}_\Delta(\tau)$  varies slowly on the scale of  $1/\Gamma$ , we may pull it out of the integral to get:

$$\mathbf{a}_\Gamma(\tau) \approx \frac{1}{\Gamma} \begin{bmatrix} 0 & \frac{e^{2i\Gamma\tau} - e^{2i\Gamma\tau_0}}{2} \\ \frac{-e^{-2i\Gamma\tau} + e^{-2i\Gamma\tau_0}}{2} & 0 \end{bmatrix} \mathbf{a}_\Delta(\tau_0). \quad (15)$$

The correction is thus suppressed by  $1/\Gamma$ , confirming that RWA is accurate when  $\Gamma \gg 1$ .

### 2. Strong Perturbation Case: $\Gamma \ll 1$

In the opposite extreme, where  $\Gamma \ll 1$ , the situation corresponds to a strong driving regime: the coupling strength  $F_0 I_{12}$  becomes comparable to or even exceeds the transition frequency  $\omega_{12}$ .

In this case, the third term in Eq. (11) becomes dynamically insignificant due to its small prefactor  $\Gamma$ , and the fourth term — a cosine modulation with fixed amplitude — dominates the dynamics.

Under these conditions, Eq. (11) simplifies to:

$$\frac{d^2}{d\tau^2} a_{1,2}(\tau) = -2(1 + \cos(2(\Gamma + \Delta)\tau)) a_{1,2}(\tau), \quad (16)$$

which leads to population oscillations of unit amplitude, but with a *time-varying frequency*. These modulated oscillations deviate significantly from the simple sinusoidal Rabi behavior predicted by RWA.

Although analytically tractable, this regime corresponds to *ultra-strong field interactions*, where the system no longer behaves as an ideal two-level model. In practice, such strong perturbations may require accounting for higher-order multipole transitions (e.g., quadrupole, octupole) or induce significant state mixing, structural distortion, or even ionization. This limits the practical utility of the resulting dynamics for coherent control applications.

### 3. Summary of the RWA Validity Criterion

Taken together, the weak-field regime characterized by

$$\Gamma \gg 1 \quad (17)$$

ensures that the counter-rotating contributions are fast-averaging and negligible, validating the RWA.

This simple condition — expressing that the drive strength is small compared to the system's transition frequency — forms the basis for the graphical Rabi spectrum method introduced in the next section.

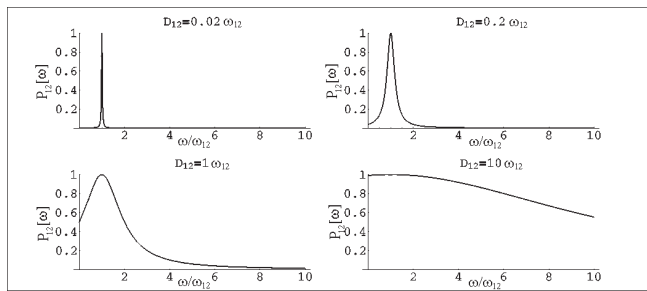


FIG. 1: Rabi profiles for a single spectral transition. The total coupling  $D_{12}$  is indicated above each graph. As  $D_{12}$  increases, the profile broadens. The horizontal axis shows the drive frequency  $\omega$  in units of the transition frequency  $\omega_{12}$ .

## III. VISUALIZING RWA VALIDITY WITH RABI PROFILES

In this section, we introduce the concept of the *Rabi profile* — a visual tool for assessing the validity of the RWA and predicting population transfer behavior in two-level and many-level quantum systems. This provides a direct graphical interpretation of the criterion  $\Gamma \gg 1$  derived in Section II.

### A. Rabi profile of a single system transition

The *Rabi profile* for a transition between levels 1 and 2 is defined as the amplitude of population oscillations predicted by the generalized RWA solution, considered as a function of the driving frequency  $\omega$ . It depends on the total coupling strength  $D_{12} \equiv F_0 I_{12}$  and the resonant transition frequency  $\omega_{12}$ , and is given by:

$$P_{12}(\omega) = \frac{1}{1 + \left(\frac{\omega - \omega_{12}}{D_{12}}\right)^2}. \quad (18)$$

This is a Lorentzian-shaped curve centered at  $\omega_{12}$ , with a half-width at half-maximum equal to  $D_{12}$  (see Fig. 1). It provides a convenient graphical means of determining whether the applied driving frequency lies in a regime where the RWA remains valid.

The validity criterion from Eq. (17) can be rephrased using the Rabi profile. Substituting  $\Gamma = (\omega + \omega_{12})/D_{12}$ , the condition  $\Gamma \gg 1$  becomes:

$$D_{12} \ll \omega + \omega_{12}. \quad (19)$$

In the worst case (i.e., driving near resonance), this reduces to:

$$D_{12} \ll \omega_{12}.$$

This means that the profile's center must lie far from the origin compared to its width — or, equivalently, that the profile has negligible height at  $\omega = 0$ .

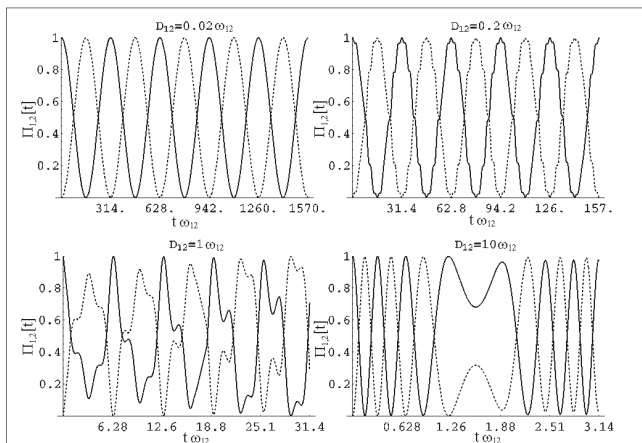


FIG. 2: Numerical solution for population dynamics of a two-level system driven at resonance. Time is shown in units of  $t\omega_{12}$ . Each subplot corresponds to a different coupling strength  $D_{12}$  (as in Fig. 1). Tick marks indicate multiples of the predicted Rabi period from Eq. (21). The full and dotted lines show  $\Pi_1(t)$  and  $\Pi_2(t)$ , respectively.

When this condition is met, the population dynamics of a two-level system driven at frequency  $\omega$  is well described by sinusoidal oscillations with amplitude:

$$A(\omega) = P_{12}(\omega) \quad (20)$$

and period:

$$T_{12}(\omega) = \frac{\pi}{D_{12}} \sqrt{P_{12}(\omega)}. \quad (21)$$

Figure 2 shows numerical solutions to the full system dynamics for a resonantly driven two-level system at increasing values of  $D_{12}$ . The Rabi profiles corresponding to each case are shown in Fig. 1. As expected, for weak coupling ( $\Gamma = 50$ ), the numerical result matches the RWA prediction exactly. As  $\Gamma$  decreases, Bloch–Siegert oscillations emerge and eventually dominate, consistent with the analysis from Section II B.

To illustrate off-resonant driving, Fig. 3 shows the same two-level system driven at four different frequencies. All share the same narrow Rabi profile (top panel), corresponding to  $D_{12} = 0.05\omega_{12}$ . Gridlines indicate the predicted amplitude and period from Eqs. (18) and (21), respectively. The numerical solutions closely follow these predictions across all cases, with deviations due to Bloch–Siegert oscillations becoming visible only in the lowest frequency cases.

## B. Many-level systems and the Rabi spectrum

The concept of a Rabi profile can be naturally extended to visualize and interpret population dynamics in more complex systems.

In this section, we introduce the idea of the *Rabi spectrum*, a graphical representation of all relevant Rabi profiles in a many-level system. We begin with the minimal

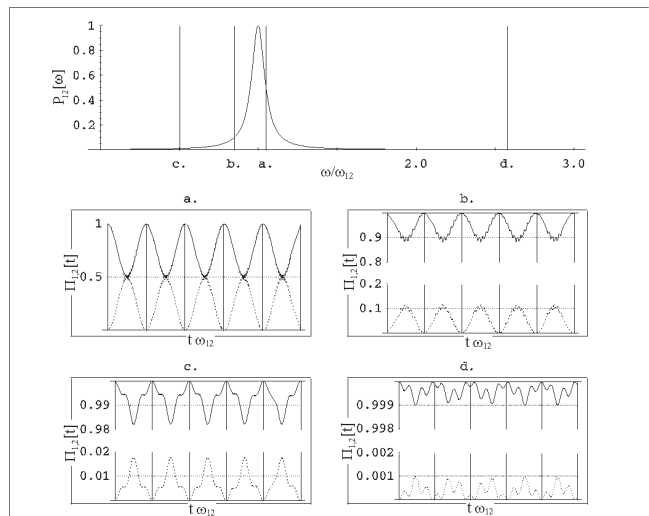


FIG. 3: Population dynamics for off-resonant driving. Top: common Rabi profile. Vertical lines indicate the four drive frequencies used. Bottom: exact numerical dynamics. Horizontal lines mark predicted amplitudes, vertical lines mark predicted periods. The agreement between RWA-based predictions and full dynamics confirms the profile’s diagnostic value.

extension — a three-level system — as it contains all the essential features from which general conclusions can be drawn.

Consider a system with three energy levels labeled 1, 2, and 3. The external drive couples levels 1 and 2 with total strength  $D_{12} = F_0 I_{12}$ , and levels 2 and 3 with strength  $D_{23} = F_0 I_{23}$ . We assume there is no direct coupling between levels 1 and 3 ( $I_{13} = 0$ ). The corresponding spectrum contains two resonant transitions:  $\omega_{12}$  and  $\omega_{23}$ .

Our goal is to transfer population from level 2 to level 1, ideally without exciting level 3. We define the *Rabi spectrum* of this targeted transition as the superposition of the individual Rabi profiles:

$$P_{12}(\omega) \text{ and } P_{23}(\omega),$$

plotted on the same frequency axis (see Figs. 4–6).

### 1. Case 1: Well-Separated, Narrow Profiles

Assume both transitions satisfy the narrow-profile condition from Eq. (19), and that the profile centers are well-separated:

$$|\omega_{12} - \omega_{23}| \gg D_{12}, D_{23}.$$

This condition can always be met by reducing the drive intensity  $F_0$ . Figure 4 (top) shows such a Rabi spectrum. The perturbation frequency is tuned to  $\omega = \omega_{12}$ , where  $P_{12}(\omega) = 1$  and  $P_{23}(\omega) \ll 1$ .

From this graphical perspective, we expect efficient population transfer between levels 2 and 1, with negligible leakage into level 3. The numerical result in Fig. 4

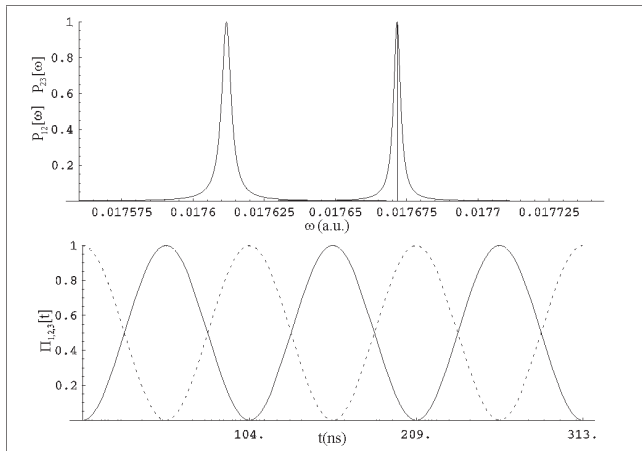


FIG. 4: Three-level system: Rabi spectrum (top) and numerical solution (bottom). The drive is tuned to  $\omega_{12}$ , and both profiles are narrow and well-separated. As predicted, the population oscillates efficiently between levels 1 and 2 with negligible excitation of level 3.

(bottom) confirms this prediction: the population oscillates cleanly between levels 1 and 2, while  $\Pi_3(t)$  remains near zero.

### 2. Case 2: Partial Spectral Overlap

Next, consider increasing the drive intensity  $F_0$  such that the profiles broaden but still satisfy Eq. (19). Now  $P_{23}(\omega_{12})$  becomes small but non-negligible. This situation is depicted in Fig. 5.

Graphically, we expect that driving at  $\omega_{12}$  will still produce strong oscillations on the  $1 \leftrightarrow 2$  transition, but some population will now be leaked to level 3 due to the nonzero value of  $P_{23}(\omega_{12})$ .

Figure 5 (bottom) confirms this: while  $\Pi_1(t)$  and  $\Pi_2(t)$  continue to exhibit robust oscillations,  $\Pi_3(t)$  now oscillates as well, with maximum amplitude approximately equal to  $P_{23}(\omega_{12})$ .

### 3. Case 3: Overlapping Profiles, Breakdown of Selectivity

If the perturbation intensity is increased further, the profiles broaden enough that the Rabi spectrum at  $\omega_{12}$  is significantly influenced by both transitions (Fig. 6). The previously dominant oscillation along  $1 \leftrightarrow 2$  is now disrupted by interference with  $2 \leftrightarrow 3$ .

The numerical result shows that  $\Pi_1(t)$  no longer follows a clean sinusoidal pattern, and  $\Pi_3(t)$  reaches substantial values. Efficient, selective transfer is no longer possible.

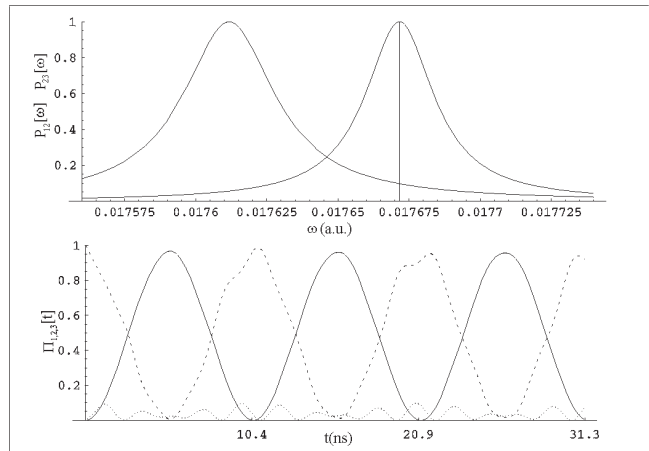


FIG. 5: Three-level system: Increased drive strength leads to broader profiles and partial spectral overlap. Some population leaks to level 3. The amplitude of  $\Pi_3(t)$  matches the height of  $P_{23}(\omega_{12})$ .

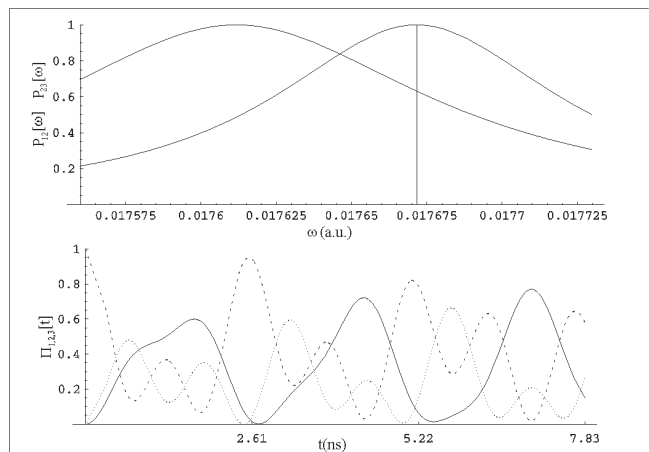


FIG. 6: Three-level system: Strong driving causes significant overlap of Rabi profiles. The targeted  $1 \leftrightarrow 2$  transition loses selectivity, and population spreads into level 3.

### 4. Conclusion: Transfer Speed Limit and the Rabi Spectrum

These examples illustrate that in any many-level system, there exists a practical upper bound to the achievable speed of efficient population transfer along a given transition. This limit is set not by external parameters, but by the system's internal structure — specifically, the spectral crowding and coupling strengths.

Let  $\alpha$  and  $\beta$  denote two levels directly coupled by the drive (i.e.,  $I_{\alpha\beta} \neq 0$ ). Efficient, high-fidelity population transfer is possible only when:

1. The Rabi profile  $P_{\alpha\beta}(\omega)$  has its center far from  $\omega = 0$ , i.e.,  $D_{\alpha\beta} \ll \omega_{\alpha\beta}$ .
2. All other profiles in the Rabi spectrum have negligible height at  $\omega = \omega_{\alpha\beta}$ .

The Rabi spectrum thus provides a fast and intuitive graphical method to assess the feasibility of selective control in complex quantum systems.

#### IV. CONCLUSION

This paper has introduced and demonstrated the use of the *Rabi spectrum* as a graphical tool for assessing the validity of the rotating wave approximation (RWA) and predicting the selectivity of population transfer in both two-level and many-level quantum systems.

The central result is a simple visual criterion for when the approximate RWA solution yields accurate dynamics: namely, that the Rabi profile for the driven transition must be narrow and well-separated from the origin, and from other transitions' profiles. When this condition is violated, additional oscillatory effects — such as Bloch–Siegert oscillations or population leakage — emerge, marking the breakdown of selectivity.

Although the mathematical derivation is straightforward, the Rabi spectrum method enables useful order-of-magnitude estimates for maximum usable drive strengths, minimal transfer times, and control limitations imposed by system structure. In practice, once the internal structure of a quantum system is known, the Rabi spectra of its allowed transitions can be computed.

This allows for rapid evaluation of which transitions support clean, high-fidelity population transfer under external driving.

Beyond individual transitions, one can imagine numerical schemes that use these spectra to search for optimal pathways through a many-level system — identifying chains of transitions that allow efficient steering of population from one target state to another, along with lower bounds on required times.

The conceptual simplicity of the Rabi spectrum method makes it particularly attractive for pedagogical use. It offers an intuitive visual explanation for complex dynamical effects and is ideally suited for teaching quantum control, introducing the rotating wave approximation, and designing laboratory experiments. As such, it can function both as a practical reference tool and as a didactic bridge to more advanced, quantitatively rigorous control theory.

Finally, this approach serves as a foundation for further analytical developments. For example, it has been shown [16] that using an optimized frequency chirp — a time-dependent variation of the driving frequency — rather than a fixed resonant drive, can further improve population transfer efficiency. These extensions highlight the potential of simple analytical frameworks to guide deeper explorations into modern quantum control.

- 
- [1] C. Benetti and D. DiVincenzo, “Quantum information and computation,” *Nature* **404**, 247–255 (2000). doi:10.1038/35005001
- [2] J. Koch *et al.*, “Charge-insensitive qubit design derived from the Cooper pair box,” *Phys. Rev. A* **76**, 042319 (2007). doi:10.1103/PhysRevA.76.042319
- [3] C. Brif, R. Chakrabarti, and H. Rabitz, “Control of quantum phenomena: Past, present and future,” *New J. Phys.* **12**, 075008 (2010). doi:10.1088/1367-2630/12/7/075008
- [4] I. I. Rabi, “Space quantization in a gyrating magnetic field,” *Phys. Rev.* **51**, 652–654 (1937). doi:10.1103/PhysRev.51.652
- [5] M. S. Shariar and P. Pradhan, “Fundamental limitation on qubit operations due to the Bloch-Siegert oscillation,” in *Proceedings of the Quantum Communication, Measurement and Computing (QCMC’02)*, arXiv:quant-ph/0212121.
- [6] J. C. A. Barata and W. F. Wreszinski, “Strong coupling theory of two-level atoms in periodic fields,” *Phys. Rev. Lett.* **84**, 2112–2115 (2000), doi:10.48550/arXiv.physics/9906029.
- [7] K. Fujii, “Two-level system and some approximate solutions in the strong coupling regime,” doi:10.48550/arXiv.quant-ph/0301145 (2003).
- [8] W.-H. Zhang, Y.-T. Zhang, M.-J. Hu, T. Chen, and G.-L. Long, “Quantum Hamiltonian learning enhanced by ancillary qubits,” *Chinese Phys. B*, vol. 33, no. 5, 050303, 2024. doi:10.1088/1674-1056/ad8a4c.
- [9] J. Hausinger and M. Grifoni, “Dissipative two-level system under strong ac driving: A combination of Floquet and Van Vleck perturbation theory,” *Phys. Rev. A*, vol. 81, 022117, 2010. doi:10.1103/PhysRevA.81.022117.
- [10] I. Pietikäinen, S. Danilin, K. S. Kumar, A. Vepsäläinen, D. S. Golubev, J. Tuorila, and G. S. Paraoanu, “Observation of the Bloch–Siegert shift in a driven quantum-to-classical transition,” *Phys. Rev. B*, vol. 96, 020501(R), 2017. doi:10.1103/PhysRevB.96.020501.
- [11] A. P. Saiko and G. G. Fedoruk, “Effect of the Bloch–Siegert shift on the frequency responses of Rabi oscillations in the case of nutation resonance,” *JETP Letters*, vol. 87, pp. 128–132, 2008. doi:10.48550/arXiv.0806.0534.
- [12] P. Forn-Díaz *et al.*, “Ultrastrong coupling regimes of light-matter interaction,” *Rev. Mod. Phys.* **91**, 025005 (2019). doi:10.48550/arXiv.1804.09275
- [13] C. Wang *et al.*, “Towards practical quantum computers: transmon qubit with a lifetime approaching 0.5 milliseconds,” *npj Quantum Information*, vol. 8, article 3, 2022. doi:10.1038/s41534-021-00510-2.
- [14] W. Demtroeder, *Laser spectroscopy: basic concepts and instrumentation*, 1st Edition, Springer-Verlag, Berlin, 1988.
- [15] F. Bloch, A. Siegert, “Magnetic resonance for nonrotating fields,” *Phys. Rev.* **57** (6) (1940) 522. doi:10.1103/PhysRev.57.522
- [16] D. Bonacci, S. D. Bosanac, and N. Došlić, “Analytic pulse design for selective population transfer in many-level quantum systems: Maximizing the amplitude of population oscillations,” *Phys. Rev. A*, vol. 70, p. 043413, 2004. https://doi.org/10.1103/PhysRevA.70.043413